AIAA JOURNAL
Vol. 44, No. 4, April 2006

Hilbert–Huang Transform Stability Spectral Analysis Applied to Flutter Flight Test Data

Norden E. Huang*
NASA Goddard Space Flight Center, Greenbelt, Maryland 20771
Martin J. Brenner†
NASA Dryden Flight Research Center, Edwards, California 93523-0273
and
Liming Salvino‡
U.S. Naval Surface Warfare Center, Carderock, Maryland 20854

A new method, the Hilbert–Huang transform (HHT), has been applied to analyze the aerostructures test wing (ATW) flight flutter data from NASA Dryden Flight Research Center. The analysis shows the yielding of the wing after the onset of flutter, but just before breaking off of the wingtip. Based on HHT, a new stability spectral analysis is also proposed that shows both positive (stable) and negative (unstable) damping. The stability spectral analysis further shows that the flutter of ATW bending occurs at 2–5 Hz in addition to 18 Hz as determined by modal analysis and identification. Both HHT and the Teager energy operator based nonlinearity indicator show that the vibrations of the ATW are nonlinear throughout the flight-test flutter maneuver.

I. Introduction

THE need for the study of airfoil aeroelastic stability becomes critical for aeroelastic design of future aircraft. Through the introduction of advanced materials and construction methods, the new approach for aeroelastic design is to have the airfoil lighter in weight with more flexibility and yet superior in performance. The consequence of such reduction in stiffness makes the structure susceptible to structural dynamics problems, specifically the onset of flutter and instability. Therefore, tools are needed to predict stability margins applicable to aeroelastic instabilities such as flutter.[1–3] Various models had been developed for this purpose. The critical step is to validate these tools and models, and the best way to carry out this validation is through flight tests. The essential problem in flight test is to determine the onset of instability from the flight data. This is an extremely challenging problem with new aeroelastic structures, and the result is critical to flight safety.[4] Pursuant to these ends, NASA Dryden Flight Research Center has conducted a total of 21 flight tests with Mach number ranging between 0.5 and 0.83 and altitudes between 10,000 ft (3050 m) and 20,000 ft (6100 m). The goal of the tests was to validate flight flutter prediction techniques.[1] Specifically, the tests addressed the following objectives: 1) generate data in response to particular excitations, 2) establish knowledge for theoretical model formulation of the flutter test system, 3) validate the accuracy of in-flight flutter predictions by providing data for the Flutterometer[2,3] and comparisons with the models, and 4) investigate the ability of engineers to monitor an experiment and safely expand the envelope near unstable flight conditions.

The aerostructures test wing (ATW) test article is a NACA 65A004 airfoil with a wing area of 97 in.^{2} (1271 cm^2) and an aspect ratio of 3.28. The wing skin is made of a three-ply fiberglass cloth 0.015 in. (0.0381 cm) thick, and the wing core is made of rigid foam. Internally, there is a spar at the 30% chord line, 1 ply 0.005-in. (0.0127-cm)-thick graphite-epoxy at its tip and 10 plies 0.05 in. (0.127 cm), thick at the root. The wing has a half-span of 18 in. (45.72 cm), a root chord of 13.2 in. (33.53 cm), and a tip chord of 8.7 in. (22.10 cm). The total weight of the wing is 2.66 lb (1.205 kg). A 15-in. (38.10-cm)-long boom 1 in. (2.54 cm) in diameter made of graphite epoxy is attached to the tip of the wing. Inside the boom are three accelerometers that are used for collecting data both on the ground and in flight testing. Each accelerometer has a range of $\pm 50g$, a sensitivity of 100 mV/g, and a frequency range from 0.3 to 12,000 Hz. The test airfoil is mounted on a flight-test-fixture (FTF), which also serves as an aircraft store consisting of a thin rectangular body with an elliptic nose and blunt tail. Its dimensions are 107 in. (2.710.813 m) in length, 32 in. (0.813 m) in depth, and 8 in. (0.203 m) in width. The electronic components for data conditioning and recording are stored in the compartment interior of the FTF, which is attached to the main pylon under the fuselage of an F-15 airplane.[4] The modal frequency of the FTF is determined to be at 200 Hz, which will have no interference with the airfoil to be tested. Details of the test are given in Ref. 4.

The designed flutter speed for ATW is near Mach 0.8. The tests for flight envelope expansion followed a standard procedure: Fly straight and level for 30 s to gather turbulence data, and then the piezoelectric excitation system on the ATW is activated and response data are recorded. During the final test, the onset of flutter was experienced at Mach 0.83 and an altitude of 3050 m (10,000 ft) when the test wing underwent violent oscillation and eventually broke near the tip. The boom and roughly 20% of the wing were lost. The whole flutter event happened over a very short period of time because the wing was destroyed within 5 s after the onset of flutter.

Past analysis of the data[4] indicates that flutter occurred for the bending mode at 18 Hz and torsion mode at 24 Hz, with a decreasing bending mode damping and an increasing torsion mode damping. The video clearly shows much larger-amplitude and lower-frequency bending motions, which is totally unaccounted for in standard analysis of the accelerometer data. Although the tests were very successful, the data analysis had always been a problem due to the transient and nonlinear properties of the wing fracturing event. No traditional method fit the requirement to analyze these data effectively because one needs a method that will take the nonstationary and nonlinear processes into full consideration. A new method, the Hilbert–Huang transform (HHT), is designed specifically for the analysis of nonstationary and nonlinear processes. The data analysis part of the test is revisited using this new data-adaptive method.

Received 14 June 2004; revision received 1 September 2005; accepted for publication 1 September 2005.

*Senior Fellow and Chief Scientist for Oceanography, Code 614.2, Laboratory for Hydrospheric and Biospheric Processes.
†Aerospace Engineer, Mail Stop 4840D, Aerostructures Branch (Code RS). Member AIAA.
‡Senior Research Engineer, Code 652, Structures and Composites, Carderock Division.

This new approach opens a new way to study nondestructive test and structural health monitoring.[5]

In this paper, results are obtained from the new approach. Also reported is a newly developed stability spectral analysis based on HHT. Before the results are reported, a brief summary of the basics of HHT is presented. Then the state of the art in vibration monitoring and damping factor computation is reviewed, followed by introduction of an improvement, the stability spectrum. The application to flutter data will follow and the main results are presented followed by a conclusions section.

(Although the Hilbert–Huang transform method is protected by patents, the software is available for personal, noncommercial, and research purposes. A license is required from NASA Goddard Space Flight Center's Technology Commercialization Office to run the software.)

II. Review of HHT

The Huang transform[6] consists of both the empirical mode decomposition and the Hilbert spectral analysis. The method was further developed in Refs. 7–10. This adaptive method is designed especially for analyzing data from nonstationary and nonlinear processes.

Traditional data analysis methods all depend on a convolution operation with a predetermined basis function set. Unfortunately, once the basis function set is selected, the convolution computation is essentially a curve fitting exercise. In addition to the limitation of the uncertainty principle, the convolution product may not produce any physically meaningful result at all. The only a priori physical interpretation is in the selection of the basis functions. For example, the selection of the trigonometric function in Fourier analysis is a tacit acceptance of a linear oscillatory system. Any nonstationarity and nonlinearity are accommodated by the harmonics. This is strictly a perturbation view of the system as discussed in Refs. 6 and 7. To accommodate the nonlinearity and nonstationarity properly, an adaptive method must be used in which the bases functions are based on and derived from the data. Based on this adaptive basis, to explore fully the effects of nonlinearity, the method will have to give us instantaneous frequency and energy with resolution power down to the intrawave frequency modulations. This immediately suggests the Hilbert transform.

For an arbitrary time series $X(t)$, its Hilbert transform $Y(t)$ is expressed as

$$Y(t) = \frac{1}{\pi} P \int \frac{X(t')}{t - t'} \, \mathrm{d}t' \tag{1}$$

where P indicates the Cauchy principal value. This transform exists for all functions of class L^p (Ref. 11). With this definition, $X(t)$ and $Y(t)$ form the complex conjugate pair, and the analytic signal $Z(t)$ results:

$$Z(t) = X(t) + iY(t) = a(t)e^{i\theta(t)} \tag{2}$$

in which

$$a(t) = \left[X^2(t) + Y^2(t)\right]^{\frac{1}{2}}$$
$$\theta(t) = \arctan\left[Y(t)/X(t)\right] \tag{3}$$

A description of the Hilbert transform with emphasis on its mathematical formality can be found in Refs. 12 and 13. Essentially, Eq. (1) defines the Hilbert transform as the convolution of $X(t)$ with $1/t$; therefore, it emphasizes the local properties of $X(t)$. In Eq. (2), the polar coordinate expression further clarifies the local nature of this representation. It is the best local fit of an amplitude and phase varying trigonometric function to $X(t)$. Even with the Hilbert transform, there is still considerable controversy in defining the instantaneous frequency as

$$\omega(t) = \frac{\mathrm{d}\theta(t)}{\mathrm{d}t} \tag{4}$$

The detailed discussions and justifications are given in Ref. 6. The limitation of the Hilbert transform on monocomponent data, however, has rendered the Hilbert transform method to be of little practical use in computing the instantaneous frequency. The real advantage of the Hilbert transform only became obvious after the empirical mode decomposition method was introduced in Ref. 6.

A. Empirical Mode Decomposition Method: Sifting Process

As discussed in Refs. 6 and 14, the empirical mode decomposition (EMD) method is necessary to deal with both nonstationary and nonlinear data. Contrary to almost all of the previous methods, this new method is intuitive, direct, a posteriori, and adaptive, with the basis of the decomposition based on and derived from the data. The decomposition is based on the simple assumption that any data consists of different simple intrinsic mode functions (IMFs) defined with the following two properties:

1) In the whole time span, the number of extrema and the number of zero crossings must either equal or differ at most by one.

2) At any point, the mean value of the envelope defined by the local maxima and the envelope defined by the local minima is zero.

Each mode response oscillation will also be symmetric with respect to the local mean. At any given time, the data may have many different coexisting modes of oscillation, one superimposed on the others.

An IMF represents a simple oscillatory mode as a counterpart to the simple harmonic function, but an IMF is much more general. With the definition, one can decompose any function by identifying all of the local extrema and connect all of the local maxima by a cubic spline line to create the upper envelope. Repeat the procedure for the local minima to produce the lower envelope. The upper and lower envelopes should cover all of the data between them. Their mean is designated as m_1, and the difference between the data and m_1 is the first component h_1, that is,[7]

$$X(t) - m_1 = h_1 \tag{5}$$

Ideally, h_1 should be an IMF because the construction of h_1 described earlier has to satisfy all of the requirements of an IMF. Yet, even if the fitting is perfect, a gentle hump on a slope can be amplified to become a local extremum in changing the local zero from a rectangular to a curvilinear coordinate system. After the first round of sifting, the hump may become a local maximum. New extrema generated in this way actually recover the proper modes lost in the initial examination. In fact, the sifting process can recover signals representing low-amplitude riding waves with repeated siftings.

The sifting process serves two purposes: to eliminate riding waves and to make the wave profiles more symmetric. Whereas the first condition is absolutely necessary for separating the intrinsic modes and for defining a meaningful instantaneous frequency, the second condition is also necessary in case the neighboring wave amplitudes have too large a disparity. Toward these ends, the sifting process has to be repeated as many times as is required to reduce the extracted signal to an IMF. In the subsequent sifting process, h_1 is treated as the data; then

$$h_1 - m_{11} = h_{11} \tag{6}$$

After repeated sifting, for example, up to k times, h_{1k} becomes an IMF, that is,

$$h_{1(k-1)} - m_{1k} = h_{1k} \tag{7}$$

then it is designated as

$$c_1 = h_{1k} \tag{8}$$

the first IMF component from the data.

Overall, c_1 should contain the finest scale or the shortest-period component of the signal. Separate c_1 from the rest of the data by

$$X(t) - c_1 = r_1 \tag{9}$$

Because the residue r_1 still contains longer-period components, it is treated as the new data and subjected to the same sifting process as described earlier. This procedure can be repeated for all of the subsequent r_j, and the result is

$$r_1 - c_2 = r_2$$
$$r_{n-1} - c_n = r_n \tag{10}$$

The sifting process can be stopped finally by any of the following predetermined criteria: either when the component c_n or the residue r_n becomes so small that it is less than the predetermined value of substantial consequence, or when the residue r_n becomes a monotonic function from which no more IMF can be extracted. Even for data with zero mean, the final residue still can be different from zero. If the data have a trend, the final residue should be that trend. By summing Eqs. (9) and (10), one finally obtains

$$X(t) = \sum_{j=1}^{n} c_j + r_n \tag{11}$$

Thus, a decomposition of the data is achieved into n empirical modes and a residue r_n that can be either the mean trend or a constant. To apply the EMD method a mean or zero reference is not required. EMD only needs the locations of the local extrema.

The components of the EMD are usually physically meaningful[8] because the characteristic scales are defined by the physical data. Additionally, a new use of the IMF components is realized, that of filtering. Traditionally, filtering is carried out based on frequency domain characteristics only. However, there is great difficulty in applying frequency-domain-based filtering when the data are either nonlinear or nonstationary, or both, because both nonlinear or nonstationary data generate harmonics for the entire frequency range. Therefore, frequency-based filtering will risk eliminating some of the harmonics, which will cause deformation of the filtered data. When IMF is used, however, time–space filtering is devised. For example, a low-pass filtered result of a signal having n IMF components can be simply expressed as

$$X_{lk}(t) = \sum_{k}^{n} c_j + r_n \tag{12}$$

high-pass results can be expressed as

$$X_{hk}(t) = \sum_{1}^{k} c_j \tag{13}$$

and a bandpass result can be expressed as

$$X_{bk}(t) = \sum_{b}^{k} c_j \tag{14}$$

The advantage of this time–space filtering is that the results preserve the full nonlinearity and nonstationarity in the physical space.

B. Hilbert Spectral Analysis

Having obtained the IMF components, one will have no difficulty in applying the Hilbert transform to each IMF component and in computing the instantaneous frequency according to Eq. (4). After the Hilbert transform is performed for each IMF component, the original data can be expressed as the real part (RP) in the following form:

$$X(t) = \mathrm{RP} \sum_{j=1}^{n} a_j(t) \exp\left[i \int \omega_j(t)\, \mathrm{d}t \right] \tag{15}$$

Here the residue r_n is left out on purpose because it is either a monotonic function or a constant. Although the Hilbert transform can treat the monotonic trend as part of a longer oscillation, the energy involved in the residual trend representing a mean offset could be overpowering. In consideration of the uncertainty of the longer trend, and in the interest of information contained in the other low-energy but clearly oscillatory components, the final non-IMF component should be left out. It could be included if physical considerations justify its inclusion.

Equation (15) gives both amplitude and frequency of each component as functions of time. The same data if expanded in a Fourier representation would be

$$X(t) = \mathrm{RP} \sum_{j=1}^{\infty} a_j e^{i\omega_j t} \tag{16}$$

with both a_j and ω_j constants. The contrast between Eqs. (15) and (16) is clear. The IMF represents a generalized Fourier expansion. The variable amplitude and the instantaneous frequency have not only greatly improved the efficiency of the expansion, but have also enabled the expansion to accommodate nonlinear and nonstationary data. With IMF expansion, the amplitude and the frequency modulations are also clearly separated. Thus, there is no restriction of the constant amplitude and fixed frequency Fourier expansion, but a variable amplitude and frequency representation is used. This frequency–time distribution of the amplitude is designated as the Hilbert amplitude spectrum, $H(\omega, t)$, or simply the Hilbert spectrum. If amplitude squared is preferable to represent energy density, then the squared values of amplitude can be substituted to produce the Hilbert energy spectrum just as well.

The skeleton Hilbert spectrum presentation is more desirable because it gives more quantitative results. Actually, Carmona et al.[15,16] have tried to extract the wavelet skeleton as the local maximum of the wavelet coefficient. Even that approach is still encumbered by the harmonics.

With the Hilbert spectrum defined, define the marginal spectrum $h(\omega)$ as

$$h(\omega) = \int_0^T H(\omega, t)\, \mathrm{d}t \tag{17}$$

The marginal spectrum offers a measure of total amplitude (or energy) contribution from each frequency value. It represents the cumulated amplitude over the entire data span in a probabilistic sense. The combination of the EMD and the Hilbert spectral analysis is also known as the HHT for short. The details of the HHT can be found in the references cited herein.

III. Present State of the Art for Damping Spectral Analysis

The present state of the art of the study of vibration characteristics in general can be found in Refs. 9 and 17 and with specific application to structural damping in Ref. 18. In spectral analysis the damping of a system is determined as follows. The vibration signals are obtained as time series from sensors strategically located in the system. The signal $x(t)$ is decomposed through the EMD part of the HHT as a sum of the IMF $c_j(t)$, given in Eq. (11). After the Hilbert transform, define the damping of the signal as

$$\gamma(t) \equiv 2\dot{\varphi}(t) = -2\left[\dot{a}(t)/a(t)\right] \tag{18}$$

the damping loss factor can be computed as

$$\eta(t) \equiv 2\zeta(t) \equiv \gamma(t)/\omega_0(t) = -[2/\omega_0(t)][\dot{a}(t)/a(t)] \tag{19}$$

where the damped frequency is

$$\omega_{0k} = \left\{ \omega_k^2(t) + [\gamma_k(t)/2]^2 \right\}^{\frac{1}{2}} \tag{20}$$

As given in Eq. (19), the damping loss factor is a function of time t and frequency ω. Reference 18 further defines the damping spectrum based on the sum of all of the squared damping loss factors as a function of time and frequency,

$$\eta^2(\omega, t) = \frac{\{[-2/a(\omega, t)][\mathrm{d}\, a(\omega, t)/\mathrm{d}t]^2\}}{\omega^2 + \{[1/a(\omega, t)][\mathrm{d}\, a(\omega, t)/\mathrm{d}t]\}^2} \tag{21}$$

They also define the root-mean-squared damping loss factor over time period T as

$$\eta(\omega, T) = \left[\frac{1}{T} \int_0^T \eta^2(\omega, t)\, \mathrm{d}t \right]^{\frac{1}{2}} \tag{22}$$

On detailed examination of the preceding description, the following key points needed generalization and improvements:

1) The damping loss factor spectrum given in Eq. (21) ignores the difference between positive damping (for stable dynamics) and negative damping (for unstable dynamics). As a result, the spectrum and the root-mean-squared valued are a mixture of critically different characteristics of stable and unstable states of the dynamic system.

2) The damping loss factor should not be computed as in Eq. (18) or (21) based on the Hilbert transform determined envelope because the envelope from the Hilbert transform has intraperiod oscillations that will give false positive as well as negative derivative values. This intraperiod frequency and amplitude fluctuation is especially pronounced for nonlinear vibrations because the intrawave frequency and amplitude modulations are indicators for nonlinearity. Unfortunately, when the vibration of the system is approaching failure, the vibration is more likely to be nonlinear; therefore, the intraperiod amplitude modulations will inevitably cause errors in the damping calculation as given in Eqs. (18) and (21). To avoid this complication, the cubic spline-fitted envelope is used, which is smoother and which lacks the intraperiod amplitude modulations.

3) The instantaneous frequency should not be computed as given in Eq. (4) from the straightforward Hilbert transform because of the limitation on the Hilbert transform imposed by Bedrosian's[19] and Nuttall's[20] theorems. A new normalized HHT (NHHT)[9] has to be used.

When the shortcomings of the present state-of-the-art method in computing the damping spectrum, is known, the concept is generalized to define a stability spectrum. This can be accomplished by using the damping computed from Eqs. (18) and (19) on the cubic spline-fitted envelope. The damping loss factor is tracked for both positive (indicating stable condition) and negative (indicating unstable condition) values, rather than Eq. (21) in which the difference between the positive and the negative signs is obliterated by the squaring operation in the definition. To define the stability spectrum, the following improvements are made over the damping spectral analysis proposed in Ref. 18: 1) Change the envelope

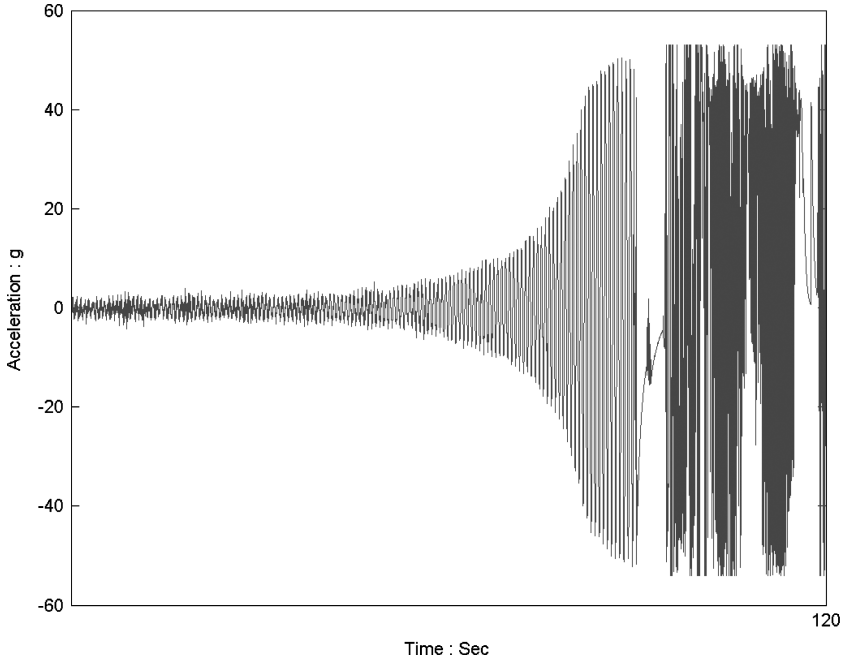

Fig. 1 ATW wingtip accelerometer response at flutter.

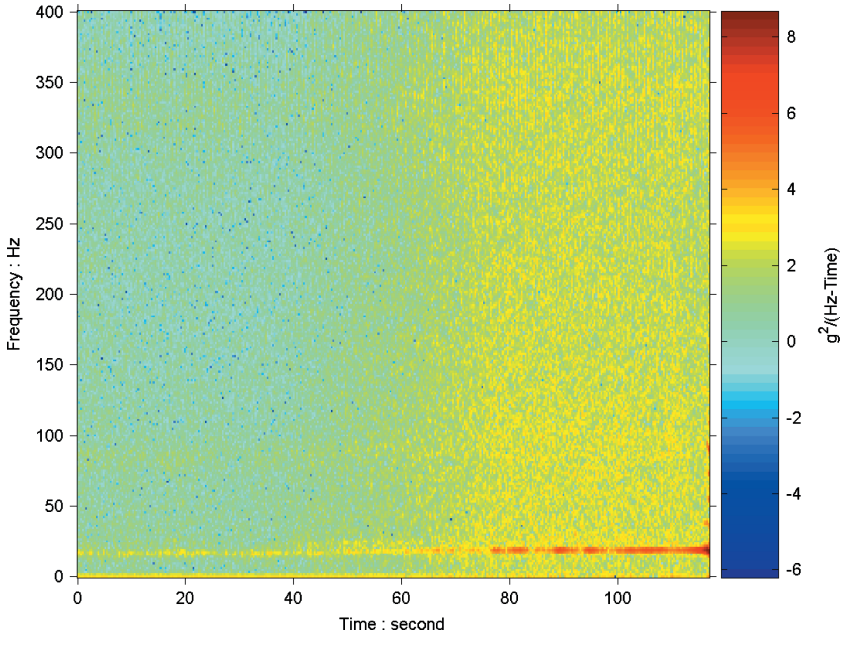

Fig. 2 Fourier spectrogram of ATW flutter data, based on 512 data point sections.

determined through Hilbert transform to cubic spline. 2) Define both positive damping (as an indication of stable dynamics) and negative damping (as an indication of unstable dynamics), and present the results accordingly. 3) Compute the instantaneous frequency using the NHHT. Also add a nonlinearity indicator through the Teager energy operator (see Refs. 21 and 22) to flag the time period when the vibration becomes nonlinear. The following two sections give detailed analysis of the ATW data.

IV. Vibration Characteristics of Flutter Data

Data from the final flutter event of the flight test is now analyzed. The wingtip accelerometer data, shown in Fig. 1, are collected from the flight test of the ATW sampled at 800 Hz. Clearly, the flutter becomes very severe immediately after its onset. The amplitude first increases exponentially, reaches a saturation stage, and eventually leads to the fracturing of the wingtip. The useful data consist only of the first 117.5 s before fracturing of the wingtip when the boom and the sensors are lost. From a simple Fourier spectrogram analysis, shown in Fig. 2, the data contain strong white noise in the latter half of the data span after the test plane accelerated to its final velocity of Mach 0.83. At the end of the data span there is also a clear indication of harmonics, suggesting that the waveform is nonlinearly distorted. To study the transition and onset of flutter, the white noise is filtered out first.

Because the sample rate is far beyond that required to analyze the flutter event, designed at 30 Hz or lower, the data are downsampled to produce eight sets of subdata at a 100-Hz sampling rate. At 100 Hz, there is still plenty of data for investigating the flutter event designed with a frequency below 30 Hz. This downsampling offers a crucial advantage: There are multisamples from a single test to give a confidence limit of the final results. Downsampling, however, has to be implemented with care, lest the aliasing overwhelm the signal. Therefore, the noise content is examined in the data before implementing filtering and the downsampling.

To study the noise content, use the EMD method to decompose the data into the IMFs given in Figs. 3a and 3b. Obviously, the eighth

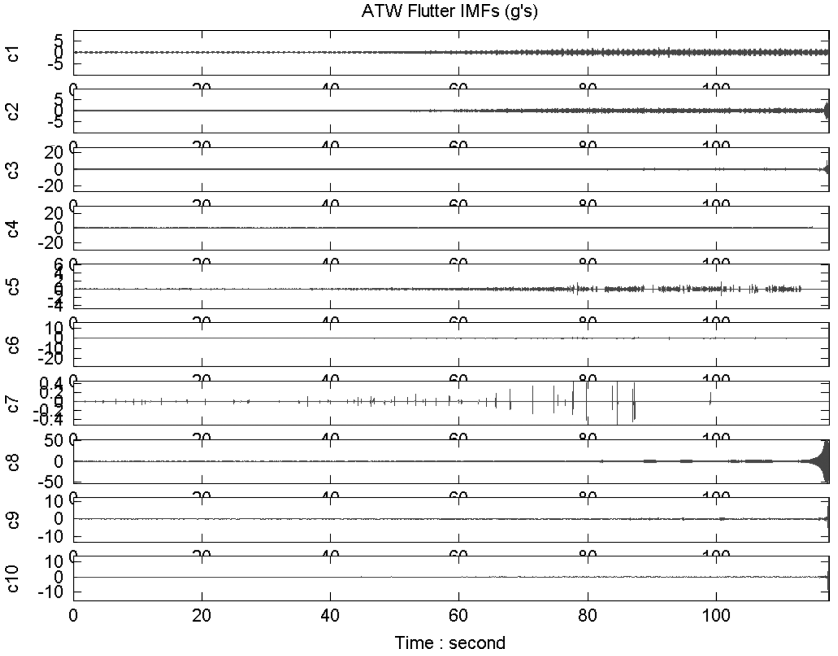

Fig. 3a First 10 IMF components from ATW flutter data.

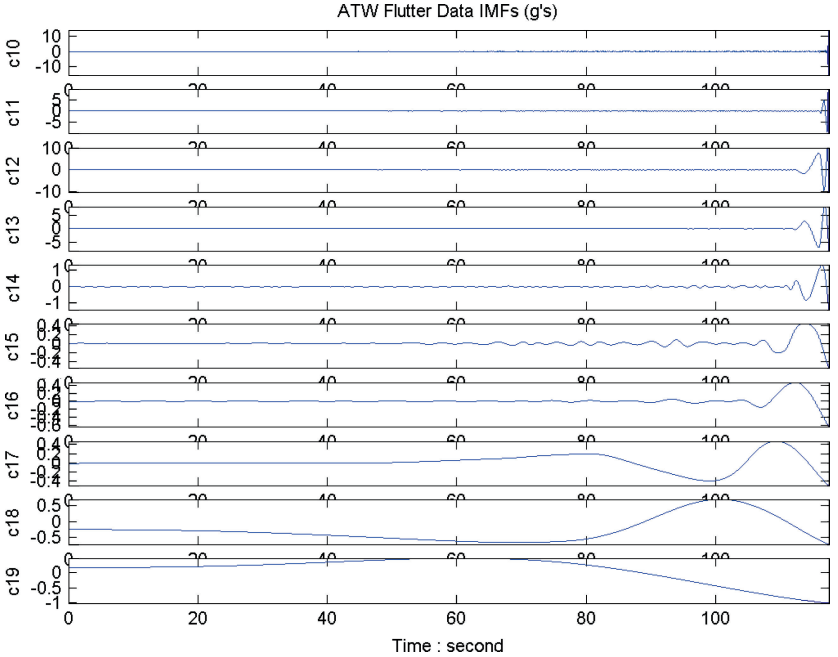

Fig. 3b Next nine IMF Components from ATW flutter data.

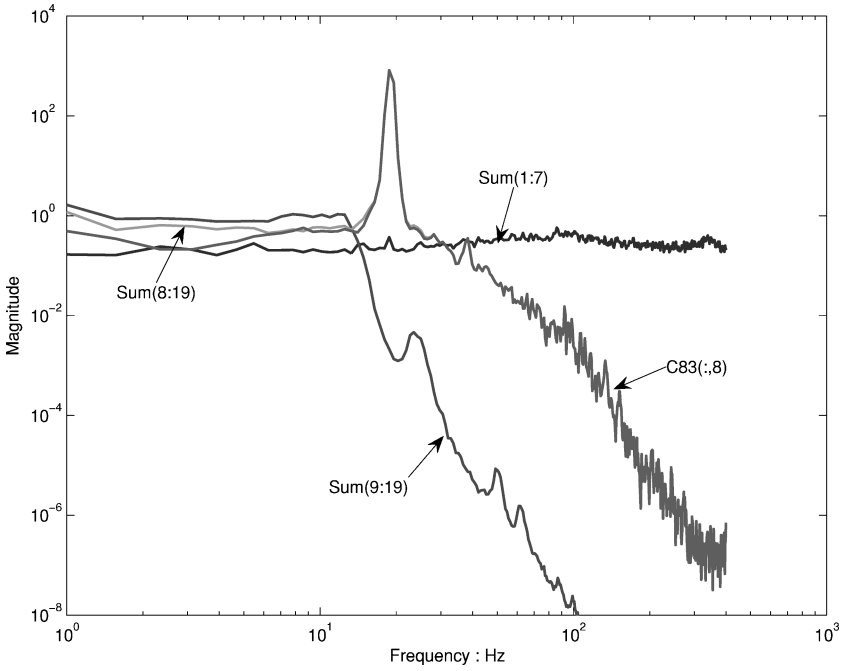

Fig. 4 Fourier spectra of various combinations of IMFs: spectrum from Sum (1:7), sum of first 7 IMFs; Sum (9:19), last 11 IMFs; Sum (8:19), last 12 IMFs; and C83 (:, 8), IMF component 8 alone.

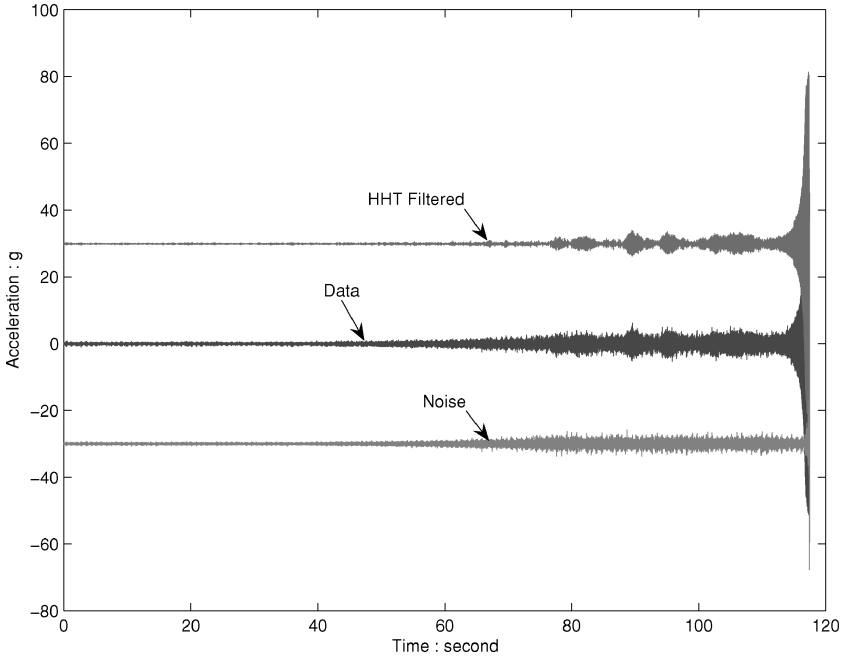

Fig. 5 Hilbert–Huang filtered data: Data, original data; HHT filtered (sum of last 12 IMFs) data; and Noise, difference (sum of first 8 IMFs) between Data and HHT filtered data.

IMF component is the most energetic with the amplitude reaching 500 g. To show the noise content, compute the Fourier power spectra for various combinations of IMFs that are given in given in Fig. 4. From these spectra, it is evident that the most energetic IMF components also carry the most critical information for the flutter study. The sum of the first seven IMF components has a nearly white spectrum. The sum of the 9th–19th IMF components represent only the low-frequency oscillations. To preserve the lower-frequency vibrations, all of the IMFs are retained from the 8th to 19th to exclude the high-frequency noise, but still retain all of the low-frequency vibrations. This operation allows for successful low-pass filtering of the data. This timescale-based filtering has been discussed in detail in Refs. 8 and 23. The advantage of the time-domain filtering is that this operation will not cause waveform distortion by removing higher harmonics associated with the low-frequency fundamentals. Because the Fourier spectrum of the sum of the first seven IMF components is essentially white, no useful information has been discarded in this HHT-based filtering. The original data, the filtered data, and the noise removed by the filtering are shown in Fig. 5.

As flutter is dominated by the vibration at around 20 Hz, our downsampling scheme should not influence the result at all, but it would provide a better mean and a confidence range of the scattering. This downsampling process produces eight subsamples; each subsample is processed to produce its Hilbert spectra. The mean of the eight Hilbert spectra is given in Fig. 6, with the corresponding marginal spectrum given in Fig. 7, together with the corresponding Fourier spectrum for comparison. By comparison, the Hilbert spectrum gives a higher dynamic range, and it also shows a

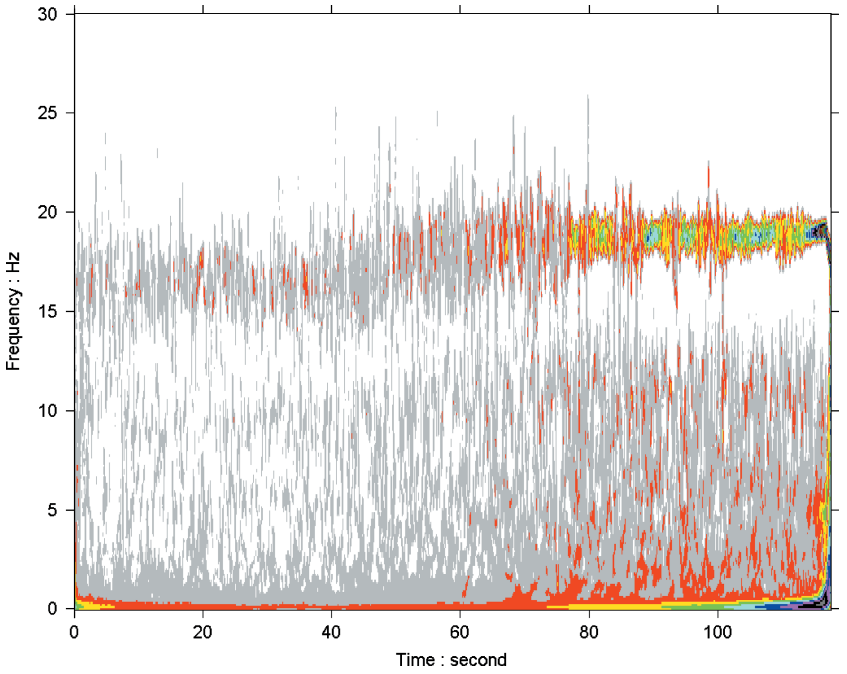

Fig. 6 Mean Hilbert spectrum from eight subsampled data sets from HHT filtered data.

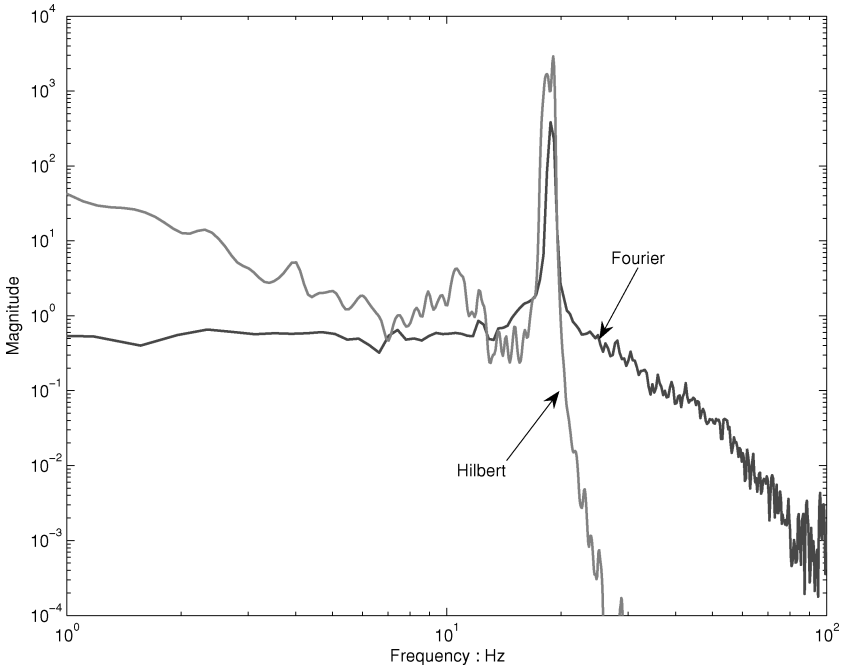

Fig. 7 Marginal Hilbert and Fourier spectra for down-subsampled data; note improved dynamic range of Hilbert over Fourier spectrum.

subharmonic peak. Crucially, the Hilbert spectrum is not encumbered by higher-frequency noise. In this case it could be from harmonics. The existence of the subharmonics indicates possible nonlinearity. Based on the subsamples, compute the detailed instantaneous frequency (IF) for the main flutter component from each subsample. The results are given in Figs. 8 and 9, with the mean and one standard deviation range also shown. The result indicates that the values obtained are very robust. The most surprising feature of the IF values is the sudden downturn near the end.

As a further comparison between the Fourier spectrogram and the Hilbert spectrum, the two are plotted together in Fig. 10. Clearly, there is a qualitative agreement. This is because the data almost satisfy the condition of loosely defined statistical stationarity. The differences are all in the details. One critical difference, for example, exists near the end of the data set. Because of the fixed data block used in computing the spectrogram, the last second cannot be evaluated with any degree of fidelity. Yet the Hilbert spectrum clearly shows some frequency anomalies there. To examine the details, the last section of the Fourier and Hilbert spectrum is expanded in Fig. 11, which shows the clear decrease of the IF as a function of time shown in Fig. 9, but it is totally absent from the spectrogram. This decrease of frequency is a crucial indication of yielding of the structure. This feature will be examined in more detail as follows.

Compute the envelopes of the data, and plot them together with the IF values for the last 1.5 s in Fig. 12. Here the decrease of the IF values coincides with the saturation of the amplitude of flutter. The amplitude no longer increases. Because the structure yields about 1 s before the final fracturing, its frequency decreases, showing the softening of the structure. Teager's energy operator is then used to process the IMF component as a nonlinear detector. In any vibration

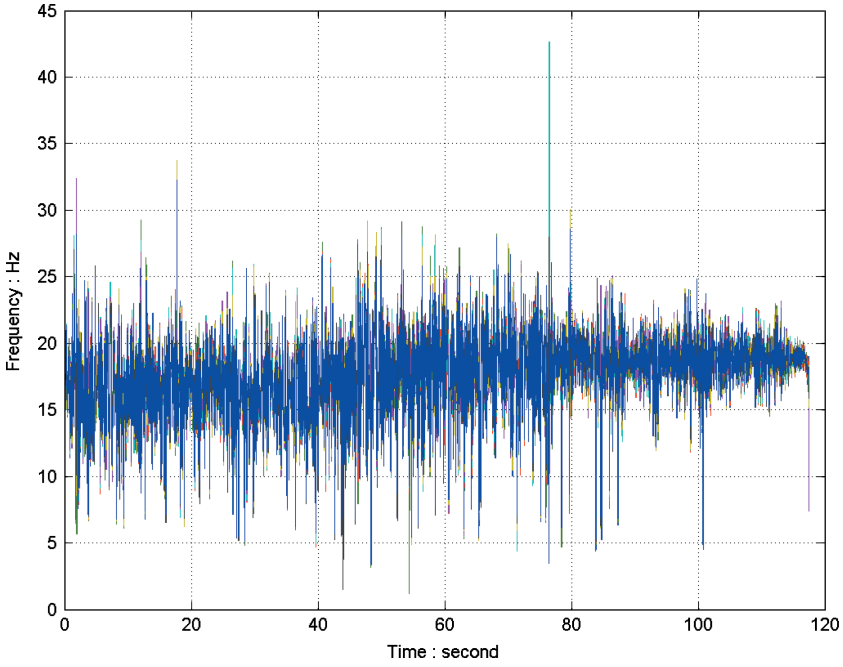

Fig. 8 IF for most energetic component of eight subsampled IMF components.

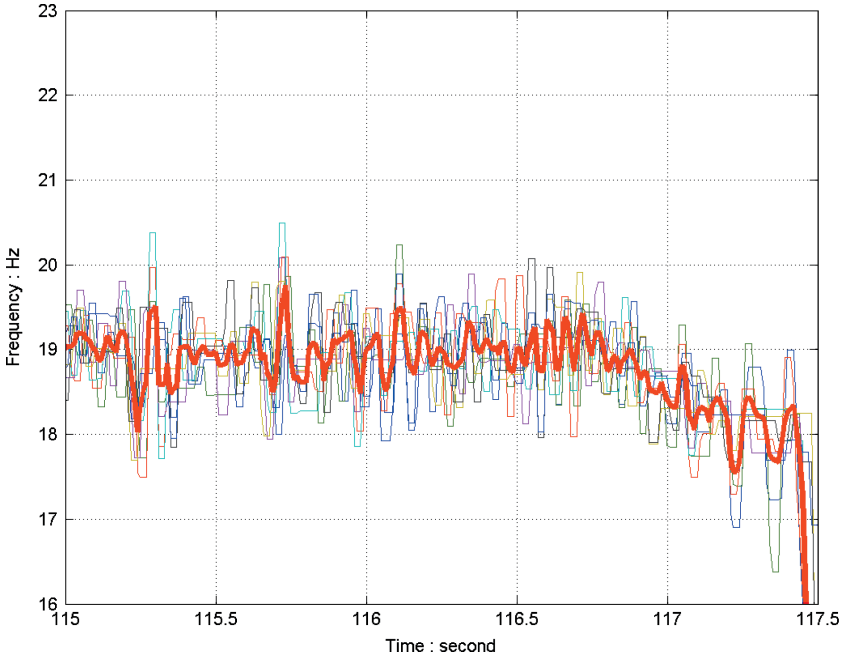

Fig. 9 Details of instantaneous frequency values for last $2\frac{1}{2}$ s from Fig. 8, eight separate values: thick red line, mean and thick dashed green line, standard deviation.

test, the presence of nonlinearity usually foretells a problem. Therefore, to identify nonlinearity in the signal is of critical importance. Intrawave frequency has been proposed[6] as a means to characterize nonlinearity. It is very useful and will still be used here. An additional method, the Teager energy operator (TEO),[24] can offer an even sharper identification of the presence of nonlinearity. The method is based on the inability of the TEO to extract instantaneous frequency from any nonlinearly distorted waveform because it is based on totally linear assumptions. Therefore, the nonlinearity indicator can be defined as the time when the instantaneous frequency becomes drastically different from the values determined by NHHT or generalized zero crossing (GZC).[24] Given some computational instability, we propose that nonlinearity is clearly present when the instantaneous frequency determined from TEO is more than a factor of two larger than the NHHT or GZC as a limit. Figure 13 gives the overall view of the IF change as a function of time. Clearly, the GZC method gives the most stable frequency because it does not take the nonlinear waveform distortion into consideration. The NHHT determined instantaneous frequency covers a wider range, indicating the existence of intrawave frequency modulations. The TEO further accentuates the existence of nonlinear waveform distortion. Therefore, the IF values show the greatest fluctuation. Obviously, most of the time the airfoil is already experiencing nonlinear vibration even though the instability is not overwhelming. Next, the stability analysis is examined using the newly developed stability spectrum analysis.

V. Stability Spectral Analysis

Vibrations in structures and machines are mostly undesirable because the result is additional stress and energy dissipation. In

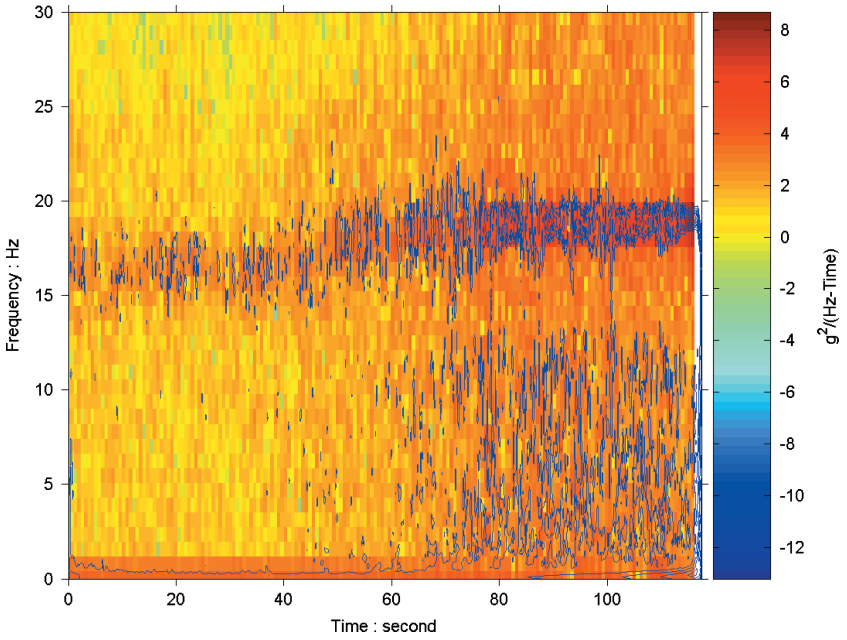

Fig. 10 Mean Hilbert spectrum (blue) and spectrogram from HHT filtered data.

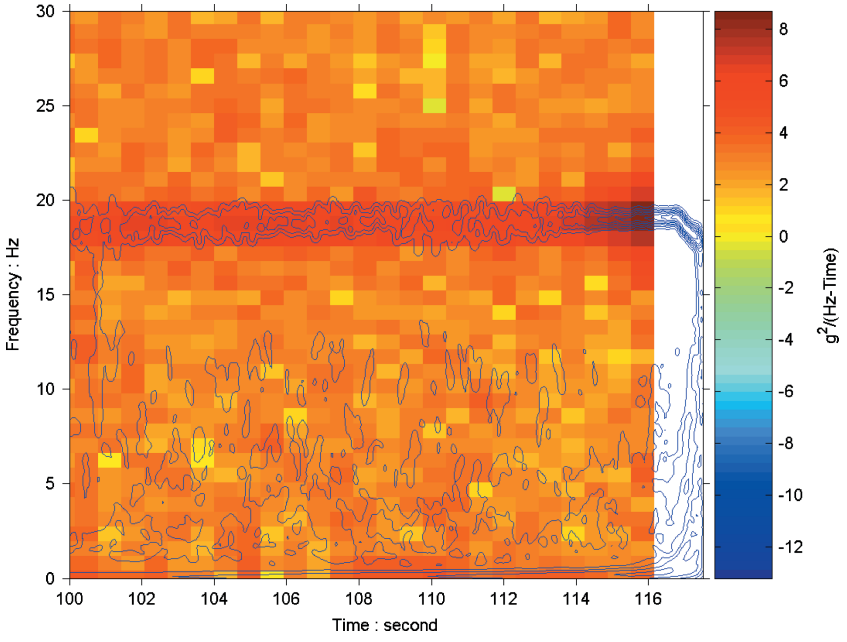

Fig. 11 Details of mean Hilbert spectrum and spectrogram from Fig. 10; note missed last second of time by spectrogram, where critical frequency downshift occurs due to structure yielding.

engineering design, various methods are used to reduce the vibration to a minimum. Unfortunately, most of the structures and machines are dynamic systems in which vibration cannot be totally avoided. Harmful as most of the vibrations are, they constitute an important part of the dynamics. Therefore, by monitoring and analyzing the vibration signal, additional information of the dynamic characteristics of the system is gained. For example, the natural frequency of a structure is related to its stiffness, and so the measured vibration frequency has been used as a diagnostic tool for determining the change of stiffness in nondestructive health monitoring.[25]

Recently, vibration signals have been used as a diagnostic tool to determine the time–frequency distribution of the damping characteristics of any dynamic system.[18] As was proposed earlier, a generalization of their approach is accomplished with a modification of the damping to study stability spectral analysis. Under unfavorable conditions, the vibrations can actually grow and even lead to failures. The renowned Tacoma Narrow Suspension Bridge was a famous example for negative damping leading to structural failure. Indeed, the vibration characteristics can be used to indicate whether the system is stable or tending toward instability. The characteristics of the vibrations can be useful indicators for operational safety criterion. The key here is the generalization of the damping definition to include both positive damping (stable) and negative damping (unstable) and the improvement of the damping computation. As discussed earlier, the current damping spectral analysis has certain shortcomings. In what follows, crucial improvements implemented recently[26] are presented. The improvements can be summarized in two critical areas.

A. Spline Envelope

As given in Eq. (18), the energy damping loss factor is determined by the time differentiation of the amplitude. In Ref. 18, the amplitude is defined as the envelope computed from the Hilbert

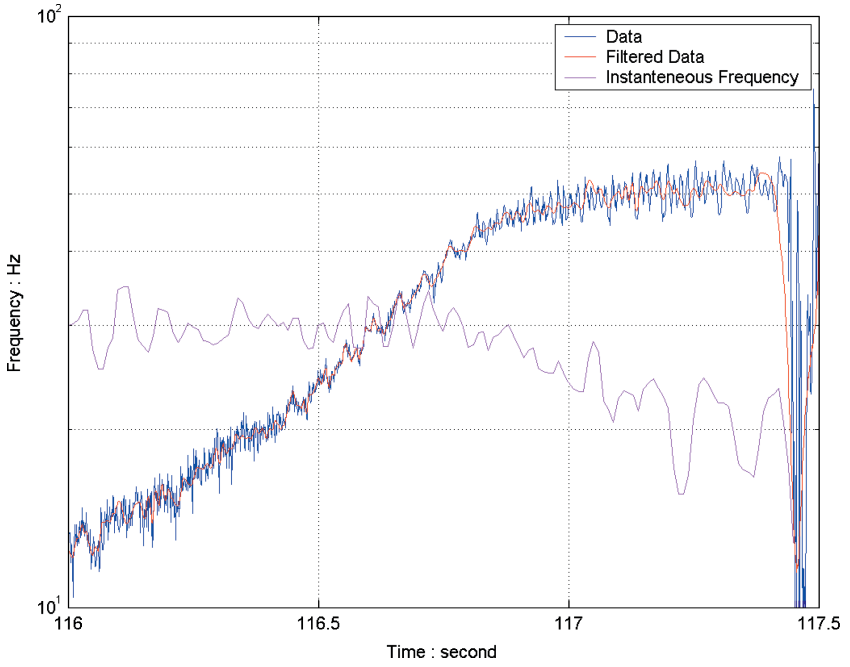

Fig. 12 Mean instantaneous frequency (magenta) and data envelope filtered (red) and unfiltered (blue); note downward trend of instantaneous frequency values as amplitude envelope levels off.

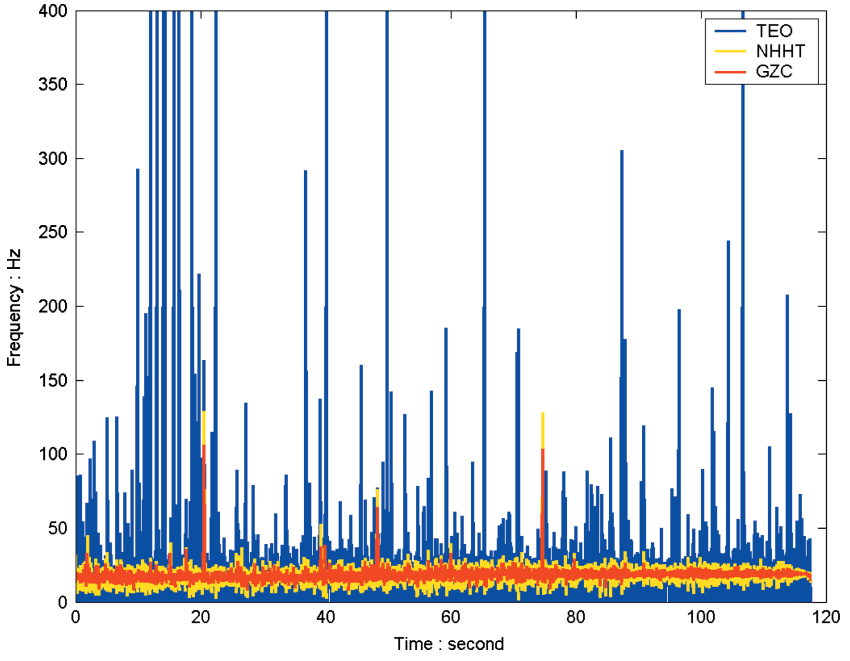

Fig. 13 IF values as determined from TEO (blue), NHHT (yellow), and GZC (red) methods for the most energetic IMF components: GZC represents mean IF; NHHT represents IF with intrawave frequency modulation; therefore, it is more variable; and TEO is based on linearity assumption, so that there are many locations where no IF is definable; as a result, TEO can be a very local nonlinearity indicator.

transform. It is well known that the Hilbert transform will show an intrawave frequency as well as amplitude modulation whenever the waveform contains nonlinear distortion. In a recent discussion on the development of the NHHT,[9] the disadvantages of using the Hilbert transform are presented for computing the envelope for data from nonlinear processes. In that instance, though the Hilbert envelope did not perform as well as the spline, the frequency determined from the Hilbert envelope normalization scheme is still acceptable. In the present case, the derivative of the amplitude is needed; therefore, any modulation of the amplitude value will give spurious values and lead to erroneous results. Let us illustrate the case by examining the flutter data as an example.

Take the most energetic component of the ATW data, as shown in Fig. 3a, and compute the amplitude envelopes from both the Hilbert transform and the cubic spline. The result is given in Fig. 14. Here the modulation of the Hilbert amplitude is very obvious because the vibration has reached the nonlinear range. Even though the amplitude fluctuation itself is not large, the time derivatives of this envelope will change sign within one wave period. When the successive difference, which is equivalent to the derivatives (to be within a constant factor of $1/\Delta t$) is taken, results are obtained as given in Fig. 15. The derivative from the Hilbert transform gives both positive and negative values with each wing oscillation. The values are two orders of magnitude higher than the spline-derived values. Note that these positive and negative flips have nothing to do with the stability. Rather, they come purely as the artifacts of the Hilbert transform when applied to nonlinearly distorted waveforms. In the past, Salvino and Cowley[18] suggested smoothing through moving

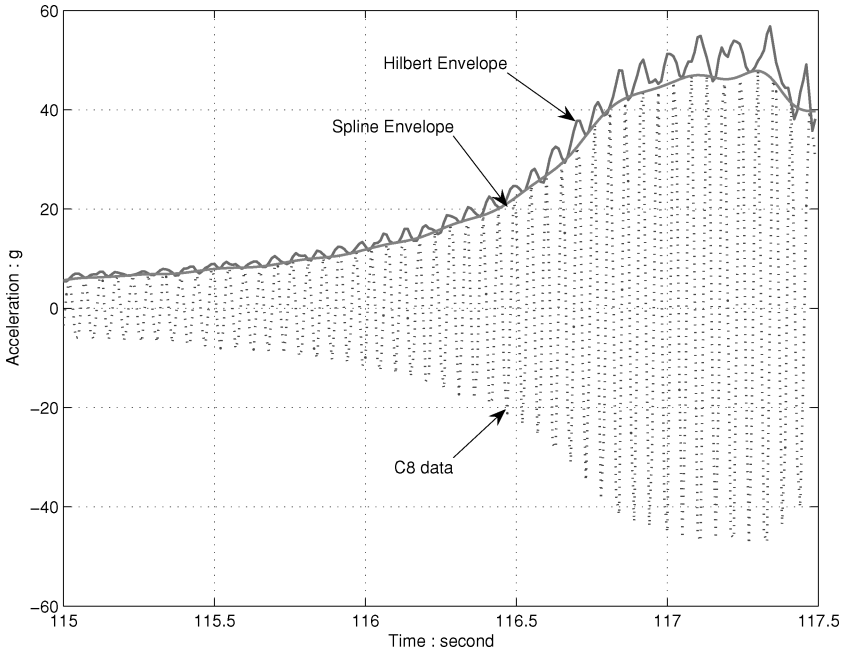

Fig. 14 Different envelopes determined from Hilbert transform and cubic spline from eighth (C8) IMF component.

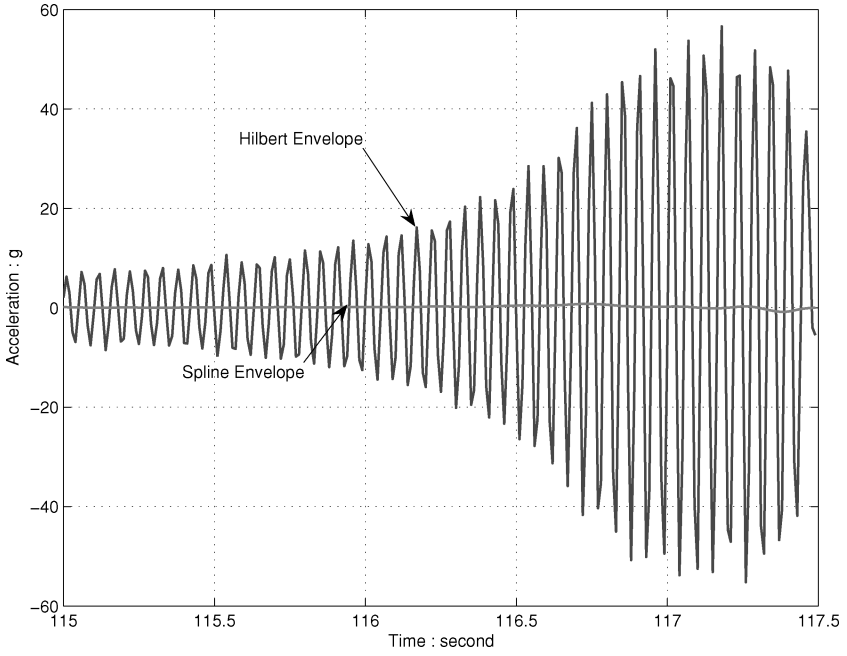

Fig. 15 Different time derivatives of envelopes, from Hilbert transform and cubic spline; note two-order-of-magnitude difference in value and alternating positive and negative derivative values of Hilbert transform envelope.

means, which can alleviate the sign flips but would never resolve the problem, whereas the derivative from the spline envelope is stable and makes perfect sense.

B. Definition of Positive and Negative Damping

The change of sign in the derivative of the spline envelope indeed represents stable and unstable vibration conditions. Therefore, the sign of the time rate of change should be retained and used as a stability indicator. The moving mean should not be computed from the positive and negative derivative to obliterate this difference. The positive and negative damping factor values should be separated into two different spectra, and the values given in Eqs. (21) and (22) are defined as the stability index. Figure 16a shows the Hilbert stability spectrum with both positive and negative damping factor registered separately. The result is produced with certain preselected parameters that will be discussed in detail presently.

Having discussed the improvements, the method is applied to flutter data. The data still need to be decomposed by EMD as in the Hilbert spectral analysis. The crucial inputs for the analysis are as follows:

1) the IMF components of the data are an M-by-N-dimensional matrix, with each column corresponding to an IMF and each row corresponding to a different time point.

2) The preselected number for the output frequency density will determine the frequency resolution of the final result.

3) The minimum frequency value for the output frequency, in which case one would select a particular frequency range for detailed examination. It should be set at zero for the initial examination.

4) The maximum frequency value in the output frequency is, again, for detailed examination and should be set as large as possible for the initial examination.

5) The initial time is a crucial input.

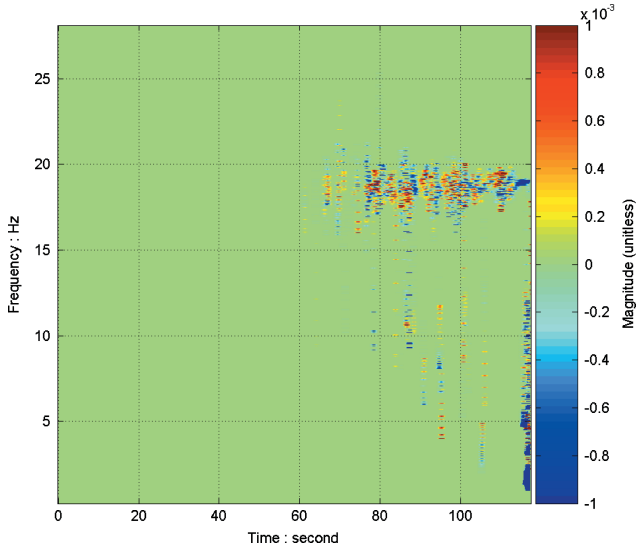

Fig. 16a Hilbert stability spectrum from ATW flutter data with cutoff limit set at 0.01 and time-average span of 10 s.

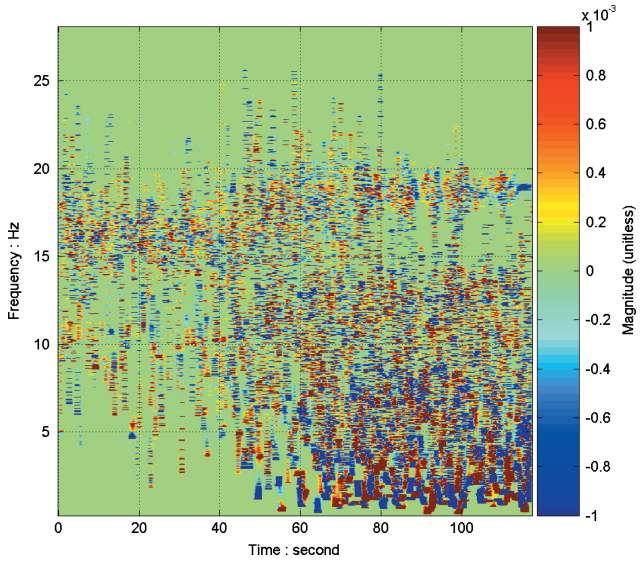

Fig. 16b Hilbert stability spectrum from flutter data with cutoff limit set at 0.001 and time-average span of 10 s; lower cutoff limit accentuates lower-amplitude components at lower frequency.

6) The final time is a crucial input.

7) The number of time points (NT) over which to smooth the resulting stability spectral values will certainly diminish resolution, but the smoothed result will give better presentation for special feature extraction and process recognition.

8) The amplitude cutoff ratio is the most crucial selection for the stability spectral analysis because the stability index depends on the ratio of the time rate of change of the amplitude to the amplitude itself. An extremely small amplitude value could produce large contributions to the resulting stability index. Yet, when the amplitude is small, its contribution to the total energy balance is negligible. This requirement is designed for a cutoff energy level to maintain a balance between different IMF components. The stability index from any oscillation with an amplitude value below the preselected percentage to the absolute maximum value is set to zero.

9) The axis scale should be preselected to generate the output frequency vector linear or log.

10) It must be decided whether to use an improved Hilbert transform to treat the ends of the data.

11) It must be decided whether to include IMF components of the IMF matrix in the Hilbert transform. One should include the last IMF component only if it is not the residual trend.

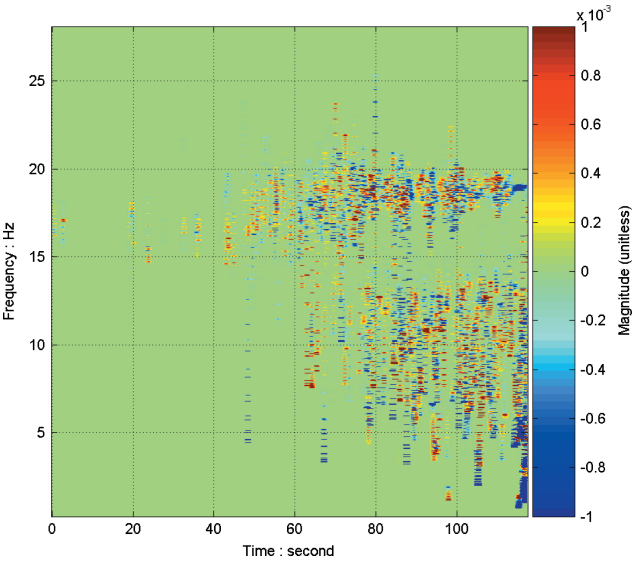

Fig. 16c Hilbert stability spectrum from flutter data with cutoff limit set at 0.005 and time-average span of 10 s; higher cutoff limit diminishes lower-amplitude components at lower frequency.

Because time differentiation will necessarily generate noise, all data are prefiltered and the resulting spectrum is smoothed over NT. Prefiltering, however, can be preselected or skipped depending on noise characteristics. One can specify the resolution of the result by selecting the number of frequency bins and the maximum and minimum values of the frequency range. The results can also be presented either in linear or logarithmic frequency scales. The data can also be pretreated to minimize the end effects in the Hilbert transformation.

Because the stability index is defined by the ratio of the derivative of the amplitude to the amplitude, its values will be dominated by the location where the amplitude is small. Yet the location with small amplitude might have too low an energy density to be of any dynamic consequence. An amplitude cutoff criterion is instituted so that the results will come from the vibrations with sufficient energy density. The resulting Fig. 16a is based on an amplitude cutoff at 0.01 with 10-point averaging. Results from other cutoff values at 0.005 and 0.001 are shown in Figs. 16b and 16c. The dramatic influence of the cutoff criterion is clearly shown. The results of the 0.001 cutoff makes the damping factor dominated by the very small amplitude at low-frequency range. It is totally due to the small value of the amplitude. These components contain a negligible amount of energy, also at the cutoff criterion of 0.005. On the other hand, if one selects this cutoff limit too high, at, for example, 0.1, one will suffer the consequence of obliterating valid information. A summary view of the effects of the cutoff limit selection is given in Figs. 17 and 18. In Fig. 17, the marginal value of the stability index is plotted as a function of frequency for various cutoff limits. Here one can see that the stability index for the cutoff limit of 0.001 is totally dominated by the low amplitude at low frequency. As the cutoff limit increases to 0.005, the stability index values begin to stabilize. In fact, the difference between 0.05 and 0.01 is quite small. If this limit is too high near 0.1, the contribution from the low-frequency end is totally obliterated.

Another view is to see the results from the marginal stability index as functions of time shown in Fig. 18. Here again, by selecting the cutoff limit at 0.001, overwhelming negative damping is produced all of the time. At the critical period just before the incipient drastic failure, all cutoff limits produce reasonable stability index values except that from 0.1. Based on this study, it is suggested that this cutoff limit be selected at 0.01.

Another less critical, yet still quite important, selection is the smoothing length NT of the final results. Visual examination reveals that too much smoothing obliterates the temporal variations. It is suggested that in future structural damping studies the stability spectral analysis be used in lieu of the originally suggested damping

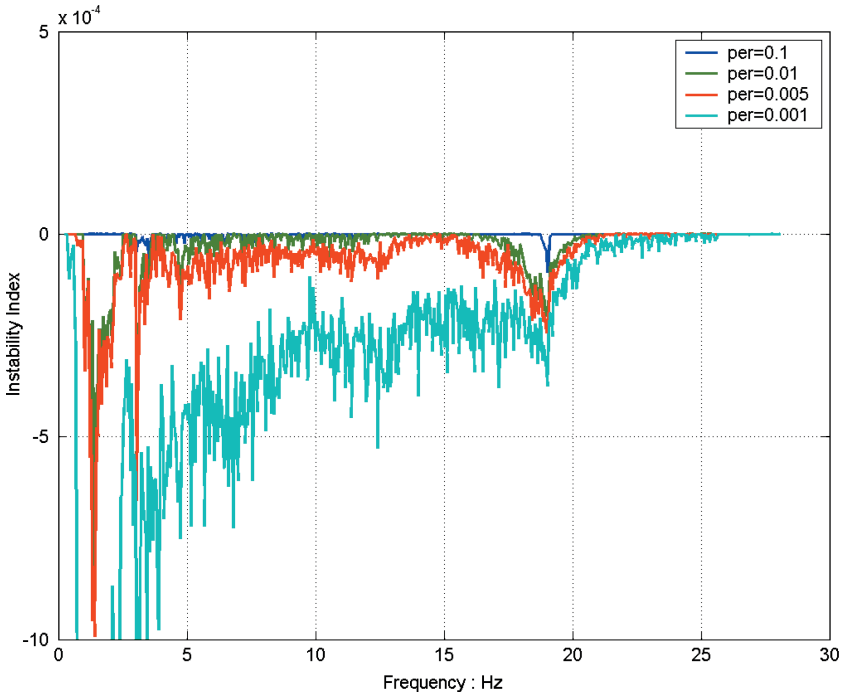

Fig. 17 Marginal stability index as function of frequency for various cutoff limits: blue, 0.1; green, 0.01; red, 0.005; and light blue, 0.001, all with time-span smoothing of 10 s; note stability index stabilized around cutoff limit between 0.05 and 0.01.

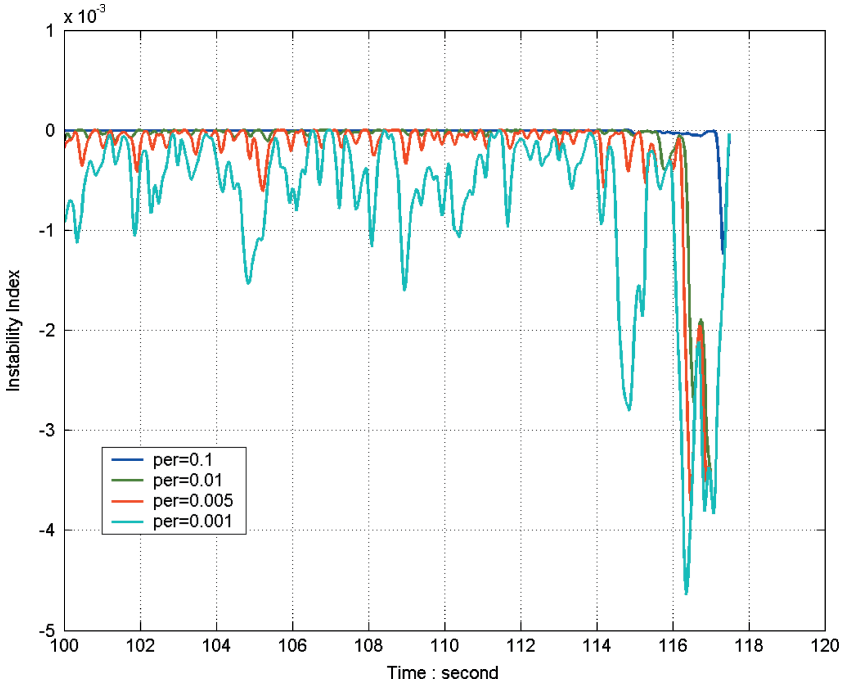

Fig. 18 Marginal stability index as function of time for various cutoff limits: blue, 0.1; green, 0.01; red, 0.005; and light blue, 0.001, all with time-span smooth of 10; note that stability index stabilized around cutoff limit between 0.05 and 0.01.

spectral analysis. The stability spectral analysis will give the same answer as the original damping spectral analysis if the vibration is linear. Otherwise, the separation of stable from unstable vibration is critical in all of the analyses.

VI. Discussion

The stability spectral analysis of the ATW flutter data indicates that the most unstable modes cover 2–5-Hz vibrations in addition to the 18-Hz vibration. Although no Fourier spectral analysis picked up any noticeable signal in this frequency range, a visual of the ATW vibration patterns before its destruction clearly shows violent large-amplitude and low-frequency oscillations in qualitative agreement with the stability spectral analysis. Because the data are from accelerometers, which accentuate the high-frequency vibrations, low-frequency vibration is examined by constructing the displacement record from the accelerometer data to confirm the results of the stability spectral analysis quantitatively. The displacement of the ATW boom at the tip of the airfoil can be computed by double integration of the acceleration data. Although integration is a noise eliminating operation in general, the slow drift from integration will totally obscure the true displacement as discussed by Huang.[27] This approach uses the HHT to remove the drift. The final detailed displacement of the wingtip as determined from the double-integrated acceleration is given in Fig. 19. Here one can see some low-frequency

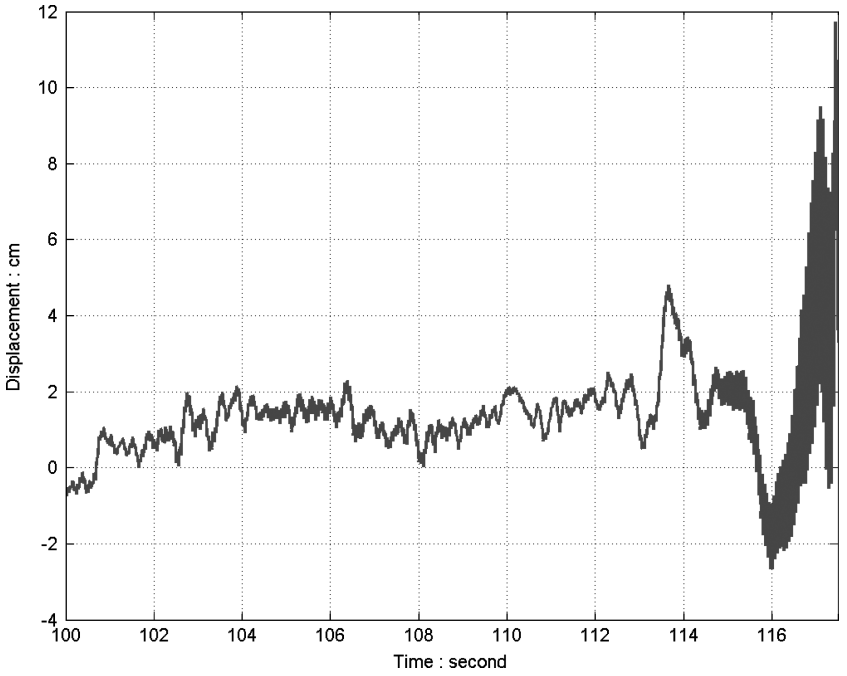

Fig. 19 Displacement of ATW wingtip computed from double integration from accelerometer data; note coexistence of large low-frequency displacement and high-frequency vibrations.

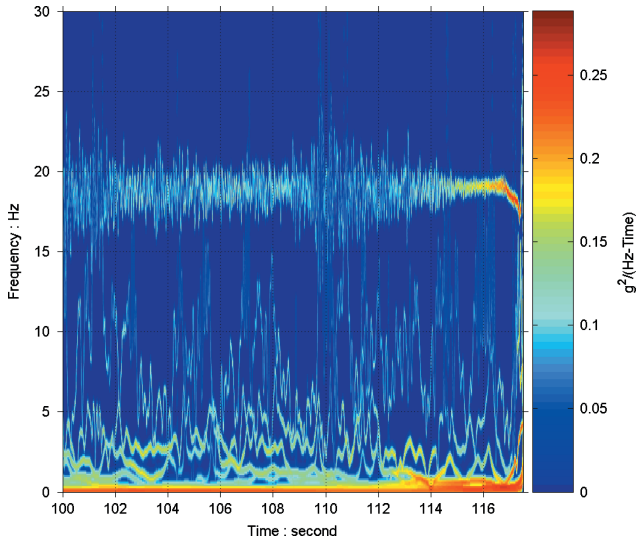

Fig. 20 Details of Hilbert spectrum for displacement of ATW wingtip; note high energy intensity at both high (18-Hz)- and low (2-Hz)-frequency regions.

displacement changes as in the visual assessment of the flutter. The high-frequency vibration is still coexisting with the much larger amplitude low-frequency vibration. The final bending just before fracture of the wing reaches almost 12 cm. The Hilbert spectrum for the displacement is given in Fig. 20. The vibration at 18 Hz is clearly shown in the Hilbert spectrum of the displacement. In addition to these high-frequency oscillations, there are low-frequency components as revealed in the stability spectral analysis, as well as the Hilbert spectrum for the displacement. For these vibration tests and stability spectral analyses, it is suggested that future data be analyzed by the methods presented.

VII. Conclusions

Based on this study, the following conclusions are drawn:

First, it has been shown that HHT can provide crucial and detailed information for studying the vibration characteristics. In the present case, HHT reveals the crucial frequency decrease, which represents the yielding of the airfoil after the onset of flutter. Because the event is highly transient, lasting for only about 1 s, a highly sophisticated and precise tool to analyze such data is needed. The frequency change at the end cannot be detected quantitatively by any method other than HHT. In addition to the final frequency decrease, HHT also reveals the stress-induced stiffening when the test wing was accelerated to the flutter speed. Although the Fourier spectrogram also indicated this event, the result is not as quantitative as HHT.

Second, it has been shown how nonlinear the flutter vibration is. The nonlinearity is revealed clearly by NHHT and TEO. Although near the end of the data, the Fourier spectrogram also shows some higher harmonics, a sure sign of nonlinearity, and no frequency downshift was visible.

Finally, the most important contribution here is the introduction of the HHT-based stability spectral analysis, which shows that the airfoil is unstable over most of the range with a negative stability index, that is, negative damping. In developing the stability spectral analysis, the Hilbert defined envelope is substituted by a cubic spline defined envelope. This is a crucial step without which the instability will be impossible for nonlinear vibrations. Because the vibrations are most likely to be nonlinear when the system is stressed to its load limit, this improvement is indeed crucial to keep both positive and negative damping factor values separate. The positive damping indicates stable, and the negative damping indicates unstable. Because the stability spectral analysis provided marginal damping factors as functions of time and frequency, it provided a crucial diagnosis tool to detect the health of the system as well. The ATW flight-test data have demonstrated that HHT can be extremely useful in analyzing vibration data and also as part of a nondestructive health monitoring system. In any future structure health monitoring system, the stability index should be a crucial component of the health indicators.

Acknowledgments

This research is supported in part by the NASA Surface Reference Technique Oceanic Processes program, U.S. Office of Naval Research Grant N0001403IP20094, and a Defense Advanced Research Projects Agency grant.

References

[1]Lind, R., and Brenner, M., *Robust Aeroservoelastic Stability Analysis,* Springer-Verlag, London, 1999.

[2]Lind, R., and Brenner, M., "Flutterometer: An On-Line Tool to Predict Robust Flutter Margins," *Journal of Aircraft*, Vol. 37, No. 6, 2000, pp. 1105–1112.

[3]Lind, R., and Brenner, M., "Flight Test Evaluation of Flutter Prediction Methods," AIAA Paper 2002-1649, April 2002.

[4]Lind, R., Voracek, D. F., Truax, R., Doyle, T., Potter, S., and Brenner, M., "A Flight Test to Demonstrate Flutter and Evaluate the Flutterometer," *Aeronautical Journal of the Royal Aeronautical Society*, Vol. 107, No. 1076, 2003, pp. 577–588.

[5]Richwine, D. M., "F-15B/Flight Test Fixture II: A Test Bed for Flight Research," NASA TM-4782, Dec. 1996.

[6]Huang, N. E., Shen, Z., Long, S. R., Wu, M. C., Shih, S. H., Zheng, Q., Tung, C. C., and Liu, H. H., "The Empirical Mode Decomposition Method and the Hilbert Spectrum for Non-Stationary Time Series Analysis," *Proceedings of the Royal Society of London, Series* A: *Mathematical and Physical Science's*, Vol. 454, No. 1971, 1998, pp. 903–995.

[7]Huang, N. E., Shen, Z., and Long, R. S., "A New View of Nonlinear Water Waves—The Hilbert Spectrum," *Annual Review of Fluid Mechanics*, Vol. 31, 1999, pp. 417–457.

[8]Huang, N. E., Wu, M. L., Long, S. R., Shen, S. S., Qu, W. D., Gloersen, P., and Fan, K. L., "A Confidence Limit for the Empirical Mode Decomposition and Hilbert Spectral Analysis," *Proceedings Royal Society of London, Series* A: *Mathematical and Physical Science's*, Vol. 459, No. 2037, 2003, pp. 2317–2345.

[9]Huang, N. E., "Empirical Mode Decomposition for Analyzing Acoustical Signal," US WO 02/065,175 A2, Patent granted 13 Feb. 2002; US 6,862,558, Patent granted 1March 2005.

[10]Wu, Z., and Huang, N. E., "A Study of the Characteristics of White Noise Using the Empirical Mode Decomposition Method," *Proceedings of the Royal Society of London, Series A: Mathematical, Physical and Engineering Sciences*, Vol. 460, No. 2046, 2004, pp. 1597–1611.

[11]Titchmarsh, E. C., *Introduction to the Theory of Fourier Integrals*, Oxford Univ. Press, Oxford, 1948.

[12]Bendat, J. S., and Piersol, A. G., *Random Data Analysis and Measurement Procedures*, 2nd Ed., Wiley, New York, 1986.

[13]Hahn, S., *Hilbert Transforms in Signal Processing*, Artech House, Boston, 1995.

[14]Huang, N. E., Long, S. R., and Shen, Z., "Frequency Downshift in Nonlinear Water Wave Evolution," *Advances in Applied Mechanics*, Vol. 32, 1996, pp. 59–117.

[15]Carmona, R., Hwang, W. L., and Torresani, B., "Characterization of Signals by the Ridges of Their Wavelet Transform," *IEEE Transactions on Signal Processing*, Vol. 45, No. 10, 1997, pp. 2586–2589.

[16]Carmona, R., Hwang, W. L., and Torresani, B., *Practical Time-Frequency Analysis: Gabor and Wavelet Transforms with an Implementation in S*, Academic Press, San Diego, CA, 1998.

[17]Huang, N. E., "Computer Implemented Empirical Mode Decomposition Method, Apparatus, and Article of Manufacture," U.S. Provisional Application Serial Number 60/023,411, 14 Aug. 1996 and Serial Number 60/023,822 filed 12 Aug. 1996; U.S. Patent 5,983,162 granted 9 Nov. 1999.

[18]Salvino, L. W., and Cawley, R., "Time-Frequency Dependent Damping Via Hilbert Damping Spectrum," U.S. Patent 6,507,798 granted 14 Jan. 2003.

[19]Bedrosian, E., "On the Quadrature Approximation to the Hilbert Transform of Modulated Signals," *Proceedings of the IEEE*, Vol. 51, May 1963, pp. 868–869.

[20]Nuttall, A. H., "On the Quadrature Approximation to the Hilbert Transform of Modulated Signals," *Proceedings of the IEEE*, Vol. 54, Oct. 1966, pp. 1458–1459.

[21]Maragos, P., Kaiser, J. F., and Quatieri, T. F., "On Amplitude and Frequency Demodulation Using Energy Operators," *IEEE Transactions on Signal Processing*, Vol. 41, No. 4, 1993, pp. 1532–1550.

[22]Maragos, P., Kaiser, J. F., and Quatieri, T. F., "Energy Separation in Signal Modulation with Application to Speech Analysis," *IEEE Transactions on Signal Processing*, Vol. 41, No. 10, 1993, pp. 3024–3051.

[23]Flandrin, P., Rilling, G., and Gonçalves, P., "Empirical Mode Decomposition as a Filterbank," *IEEE Signal Processing Letters*, Vol. 11, No. 2, 2003, pp. 112–114.

[24]Huang, N. E., Wu, Z., Long, S. R., Arnold, K. C., Blank, K., and Liu, T. W., "On Instantaneous Frequency," *Proceedings of the Royal Society of London* (submitted for publication).

[25]Huang, K., "Structure Safety Inspection," U.S. Patent 6,192,758, granted 27 Feb. 2001.

[26]Huang, N. E., and Salvino, L., "Stability Spectrum for Structural Members Through Hilbert–Huang Transform," GSC 14,833-1, Application 60/533914, U.S. patent pending, 2003.

[27]Huang, N. E., Chern, C. C., Huang, K., Salvino, L., Long, S. R., and Fan, K. L., "Spectral Analysis of the Chi-Chi Earthquake Data: Station TUC129, Taiwan, Sept. 21, 1999," *Bulletin of the Seismological Society of America*, Vol. 91, Oct. 2001, pp. 1310–1338.

H. Reed
Associate Editor

Color reproductions courtesy of NASA Dryden Flight Research Center.